Available online at www.sciencedirect.com
ScienceDirect
Ceramics International 34 (2008) 1811–1817
CERAMICS INTERNATIONAL
www.elsevier.com/locate/ceramint

Elastic properties of spark plasma sintered (SPSed) ZrB_2–ZrC–SiC composites

Shuqi Guo [a,*], Yutaka Kagawa [a,b], Toshiyuki Nishimura [c], Hidehiko Tanaka [c]

[a] *Composites and Coatings Center, National Institute for Materials Science, 1-2-1 Sengen, Tsukuba, Ibaraki 305-0047, Japan*
[b] *Research Center for Advanced Science and Technology, The University of Tokyo, 4-6-1 Komaba, Meguro-ku, Tokyo 153-8505, Japan*
[c] *Nano Ceramic Center, National Institute for Materials Science, 1-1 Namiki, Tsukuba, Ibaraki 305-0044, Japan*

Received 12 February 2007; received in revised form 18 May 2007; accepted 17 June 2007
Available online 10 August 2007

Abstract

This study investigates the elastic moduli of ZrB_2–ZrC–SiC (ZZS) composites with or without AlN and Si_3N_4 additives consolidated by spark plasma sintering. The effect of the additives on the properties is assessed. The soundwave velocities in the longitudinal and transverse modes were measured. The elastic moduli were calculated from the sound velocities and densities. The results indicate that the elastic moduli of ZrB_2–ZrC–SiC materials depend on additives and porosity. This dependence is described by a linear relation between the elastic moduli and the longitudinal soundwave velocity. The obtained elastic moduli of the fully dense ZrB_2–ZrC–SiC materials with AlN and Si_3N_4 additives are the following: $E = 459$ GPa, $G = 196$ GPa, $\nu = 0.17$ for ZZS, $E = 418$ GPa, $G = 178$ GPa, $\nu = 0.18$ for ZZS + AlN, and $E = 462$ GPa, $G = 197$ GPa, $\nu = 0.17$ for ZZS + Si_3N_4.

Keywords: ZrB_2–ZrC–SiC composites; Elastic moduli; Spark plasma sintering; Soundwave velocity; Si_3N_4 and AlN additives

1. Introduction

Diborides of zirconium (ZrB_2)-based composites have extremely high melting point (>3000 °C), high thermal and electrical conductivities, chemical inertness against molten metals, and great thermal shock resistance [1,2]. These unique mechanical and physical properties have never been achieved by other ceramics materials, e.g. Al_2O_3, ZrO_2, Si_3N_4, and SiC. Thus, the ZrB_2-based composites have become an important class of materials for structural applications at ultra high temperatures. Recently, the ZrB_2-based ceramics composites are being considered for use as potential candidates for a variety of high-temperature structural applications, including furnace elements, plasma-arc electrodes, or rocket engines and thermal protection structures for leading-edge parts on hypersonic re-entry space vehicles at over 1800 °C [1–5].

The major problems encountered with ZrB_2-based ceramics composites involve densification [6] and high temperature oxidation [7,8]. Sintering of pure ZrB_2 ceramics to full density is difficult because the low self-diffusivity of the covalent material does not allow densification by classical solid-state sintering technique. To improve sinterability, nitrides, like AlN, Si_3N_4, ZrN, are added to pure ZrB_2 [9–11], producing the formation of an intergranular secondary phase that aids the densification of ZrB_2. In addition, spark plasma sintering (SPS) is one the most recent processing techniques developed for densifying ceramic materials, including poorly sinterable compounds [12,13]. Previous studies in ZrB_2-based ceramic materials showed that SPS enhanced densification and refined microstructure in very short processing cycles [14,15]. This is attributable to the presence of the electrical field during SPS which caused faster diffusion due to the enhanced speed migration of ions [16].

Recently, the fully dense ZrB_2-based composites with AlN and Si_3N_4 additives were consolidated by hot-pressing and/or spark plasma sintering, and the obtained composites showed high flexural strength and good fracture toughness as well as high oxidation resistance [9,14,15,17]. This shows that AlN and Si_3N_4 are the suitable additives for improving the sinterability as well as the flexural strength of pure ZrB_2 ceramics. However,

* Corresponding author. Tel.: +81 29 859 2223; fax: +81 29 859 2401.
E-mail address: GUO.Shuqi@nims.go.jp (S. Guo).

0272-8842/$34.00
doi:10.1016/j.ceramint.2007.06.010

the elastic properties of ZrB_2-based ceramic materials are little known. In particular for the ZrB_2-based materials consolidated by SPS, the elastic properties and the effect of additive remain to be seen. The elastic properties are one the important mechanical properties of the ZrB_2-based ceramic materials for structural design, and they are closely linked with composition, microstructure and additives. Therefore, it is important to learn the elastic properties of the ZrB_2-based ceramic materials and the effects of AlN and Si_3N_4 additives on these properties. In this study, the ZrB_2–ZrC–SiC composites with AlN and Si_3N_4 additives were consolidated by spark plasma sintering. The microstructure was characterized by field emission scanning electron microscopy. The elastic properties of the obtained composites were measured by using ultrasonic measurements. Also, the effects of additives and porosity on the elastic properties of the composites were discussed.

2. Experimental procedure

2.1. Materials

The starting materials used in this work are commercially available ZrB_2 (Grade F, Japan New Metals Co., Ltd., Tokyo), ZrC (Grade F, Japan New Metals Co., Ltd., Tokyo), SiC (Grade UF-25, H.C. Starck, Berlin, Germany), α-rich Si_3N_4 (SN-E10, UBE Industries, Tokyo, Japan), AlN (Grade E, Tokuyama Soda Co., Tokyo, Japan). Three batches of powder were wet mixed, one containing 26.18 wt.% ZrB_2, 59.87 wt.% ZrC and 13.95 wt.% SiC, other two adding 5 wt% AlN and 5 wt.% Si_3N_4 additives, respectively, in order to assess the effect of the additive. The compositions for each material are shown in Table 1. The mixing was conducted in ethanol for 24 h using SiC milling media. The mixtures were then dried using a rotation evaporator. Before sintering, the dried mixtures were sieved through a metallic sieve with −60 mesh screen size. The powder mixture was put into graphite die lines with graphite foil and sintered using DR. Sinter (SPS-1030, Simitomo Coal Mining Co. Ltd., Tokyo, Japan). The sintering was performed at different temperatures between 1700 °C and 1900 °C for 5 min in argon atmosphere, using a heating rate of ∼430 °C/min and a pressure of 30 MPa. Changes in temperature and sintering displacement were recorded by a computer during the entire sintering process. Final sintered specimen size was 15 mm diameter pellets with a thickness of ∼3.0 mm.

The density, ρ, of the composites was evaluated by the Archimedes method with distilled water as medium. The sintered composite pellets were then polished with a diamond paste up to 0.5 μm. The morphology of the composites microstructure was characterized by field emission scanning electron microscopy (FE-SEM), and the crystalline phase compositions were identified by X-ray diffractometry (XRD). Hereafter, the three series of ZrB_2–ZrC–SiC compositions compacts are denoted as ZZS, ZZS + AlN, and ZZS + Si_3N_4, respectively.

Table 1
Compositions of the three composites used in this study

Samples	Compositions (wt.%)				
	ZrB_2	ZrC	SiC	AlN	Si_3N_4
ZZS	26.18	59.87	13.95	0	0
ZZS + AlN	24.87	56.88	13.25	5.00	0
ZZS + Si_3N_4	24.87	56.88	13.25	0	5.00

2.2. Measurement of elastic properties

The elastic moduli measurements of the composites were determined using ultrasonic equipment (TDS 3052B, Tektronix Inc. Beaverton, OR, USA) with a fundamental frequency of 20 MHz. Young's modulus, E, shear modulus, G, and Poisson's ratio, ν, are given by [18,19].

$$E = \rho V_t^2 \left(\frac{3V_l^2 - 4V_t^2}{V_l^2 - V_t^2} \right) \quad (1)$$

$$G = \rho V_t^2 \quad (2)$$

$$\nu = \frac{E}{2G} - 1 \quad (3)$$

where ρ is the density, V_l and V_t are the longitudinal and transverse soundwave velocities, respectively. V_l and V_t are determined by

$$V_l = \frac{2h}{\Delta t_l} \quad (4)$$

$$V_t = \frac{2h}{\Delta t_t} \quad (5)$$

where h is the specimen thickness, Δt_l and Δt_t are the elapsed times between the pulse and the echo of the longitudinal and transverse waves, respectively. The accuracy of the soundwave velocity measurement was better than 1%.

3. Results and discussions

3.1. Densification behavior

In Fig. 1, typical examples of the shrinking curves obtained during the SPS cycle for the three compositions are

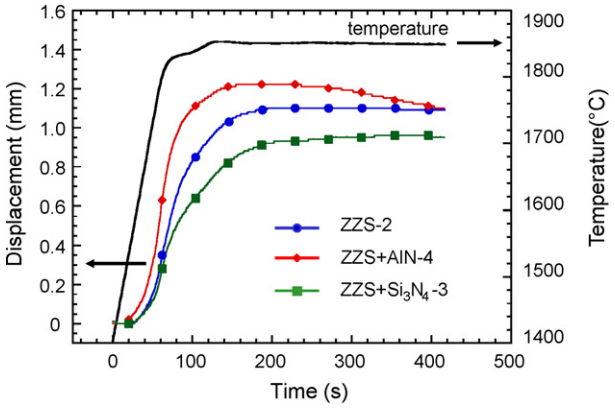

Fig. 1. Shrinking curves of the three composites consolidated by SPS at 1850 °C during the SPS cycle.

presented. The densification process of the three composites progressed very rapidly. Once activated, the densification was completed within a narrow temperature interval ranging from 1500 °C to 1900 °C. This means that the densification was completed within ~2 min. The onset temperature of densification, at which a measurable shrinkage behavior is observed, was approximately 1580 °C for the ZZS powder. The onset temperature of densification for the ZZS + Si_3N_4 powder was ~1550 °C, whereas in the case of the ZZS + AlN powder this temperature was about 100 °C lower than that of ZZS. This suggests that AlN additive was more effective for lowering the onset temperature of densification of ZZS than Si_3N_4 additive. In addition, the three compositions show nearly the same shrinking rate at the initial stage of densification, regardless of the additives. However, the shrinking rate is different at the later stage of densification depending on the additives, and the rate has the order ZZS + AlN > ZZS > ZZS + Si_3N_4. These observations indicated that the AlN additive lowered the onset temperature of densification as well as maintained the high shrinking rate, while the Si_3N_4 additive lowered only the onset temperature of densification. Thus, the AlN additive is more effective for promoting densification of ZrB_2-based composites than the Si_3N_4 additive.

The measured densities for the three composites materials consolidated by SPS between 1700 °C and 1900 °C are summarized in Table 2. The theoretical densities of the composites were calculated according to the rule of mixtures. From this table, it is found that the relative densities exceeding 95% were obtained at 1800 °C for the ZZS + AlN powder, and at 1850 °C for both the ZZS and ZZS + Si_3N_4 powders with a holding time of 5 min under a pressure of 30 MPa. This indicated that the AlN additive significantly accelerated the densification of the ZrB_2–ZiC–SiC composite during the sintering. The Si_3N_4 additive, although promoted the densification, was not more effective than the AlN additive. This is consistent with the previous observations reported by Monteverde and Bellosi [9,11], who showed nearly-fully dense ZrB_2 compacts with AlN and Si_3N_4 hot-pressed between 1750 °C and 1850 °C.

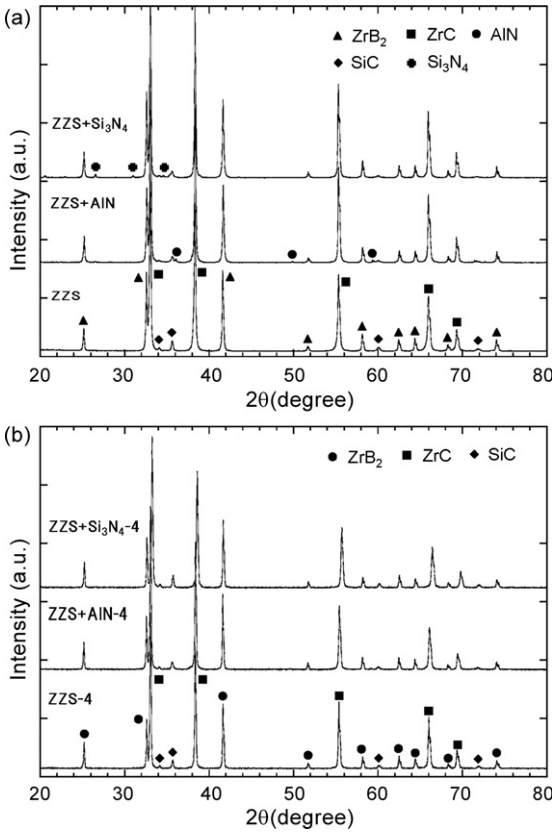

Fig. 2. X-ray diffractions of the three composites consolidated by SPS, (a) before sintering, and (b) after sintering.

3.2. Microstructural characterization

The phase contents of the mixture powders after the milling and the composite compacts consolidated by SPS were examined by X-ray diffraction; some examples are shown in Fig. 2. In the case of the mixture powders (Fig. 2(a)), the crystalline phases consisted of ZrB_2, ZrC and α-SiC for the ZZS composition, ZrB_2, ZrC, α-SiC, and AlN for the ZZS + AlN composition, ZrB_2, ZrC, α-SiC and α-Si_3N_4 for the ZZS + Si_3N_4 composition. This means that after 24 h mixing the phase of the starting powders did not

Table 2
Densities, soundwave velocities and elastic properties measured in the three composites consolidated by SPS

Samples	Processing conditions	Theoretical density (g/cm^3)	Measured density (g/cm^3)	Relative density (%TD)	Soundwave velocity (m/s)		Elastic properties		
					V_l	V_t	G (GPa)	E (GPa)	
ZZS-1	1800 °C/30 MPa/5 min	5.68	5.19	91.5	8604	5450	154	360	0.17
ZZS-2	1850 °C/30 MPa/5 min	5.68	5.46	96.1	9125	5678	176	417	0.18
ZZS-3	1875 °C/30 MPa/5 min	5.68	5.57	98.1	9132	5756	185	432	0.17
ZZS-4	1900 °C/30 MPa/5 min	5.68	5.67	99.9	9326	5876	196	459	0.17
ZZS + AlN-1	1700 °C/30 MPa/5 min	5.47	4.65	84.9	7344	4545	96	228	0.19
ZZS + AlN-2	1750 °C/30 MPa/5 min	5.47	4.92	89.9	8177	5045	125	299	0.19
ZZS + AlN-3	1800 °C/30 MPa/5 min	5.47	5.34	97.7	8974	5630	170	398	0.18
ZZS + AlN-4	1850 °C/30 MPa/5 min	5.47	5.44	99.5	9115	5713	178	418	0.18
ZZS + Si_3N_4-1	1700 °C/30 MPa/5 min	5.50	4.57	83.2	7911	4883	109	260	0.19
ZZS + Si_3N_4-2	1750 °C/30 MPa/5 min	5.50	4.92	89.5	7808	5000	123	284	0.17
ZZS + Si_3N_4-3	1850 °C/30 MPa/5 min	5.50	5.25	95.4	9219	5762	174	411	0.18
ZZS + Si_3N_4-4	1900 °C/30 MPa/5 min	5.50	5.52	100	9481	5798	197	462	0.17

changed. After SPS (Fig. 2(b)), X-ray analysis revealed the reflections of ZrB_2, ZrC, α-SiC for the three compositions. However, traces of neither AlN nor α-Si_3N_4 could be detected for the ZZS + AlN and the ZZS + Si_3N_4 compositions. This suggests that AlN and α-Si_3N_4 disappeared after SPS due to reaction although an appreciable amount of any other crystalline phases was not detected for both the ZZS + AlN and the ZZS + Si_3N_4 composites.

In Fig. 3, typical FE-SEM images of the three compositions consolidated by SPS are presented. A homogeneous microstructure was observed for the three compositions consolidated by SPS at 1850 °C and 1900 °C, and porosity is almost absent. SEM-EDX analysis shows that the BN is present between the ZrB_2 and the SiC grains for the ZZS + AlN and the ZZS + Si_3N_4 compositions, but no other product was observed for the ZZS composition. The presence of BN in the ZrB_2-based ceramics with AlN and Si_3N_4 additives is well documented in the literature. Monteverde and Bellosi [9,11] showed the presence of BN in the hot-pressed ZrB_2 with AlN and Si_3N_4 additives, as a result of the reaction of B_2O_3 with AlN and Si_3N_4 during sintering according to the following reactions:

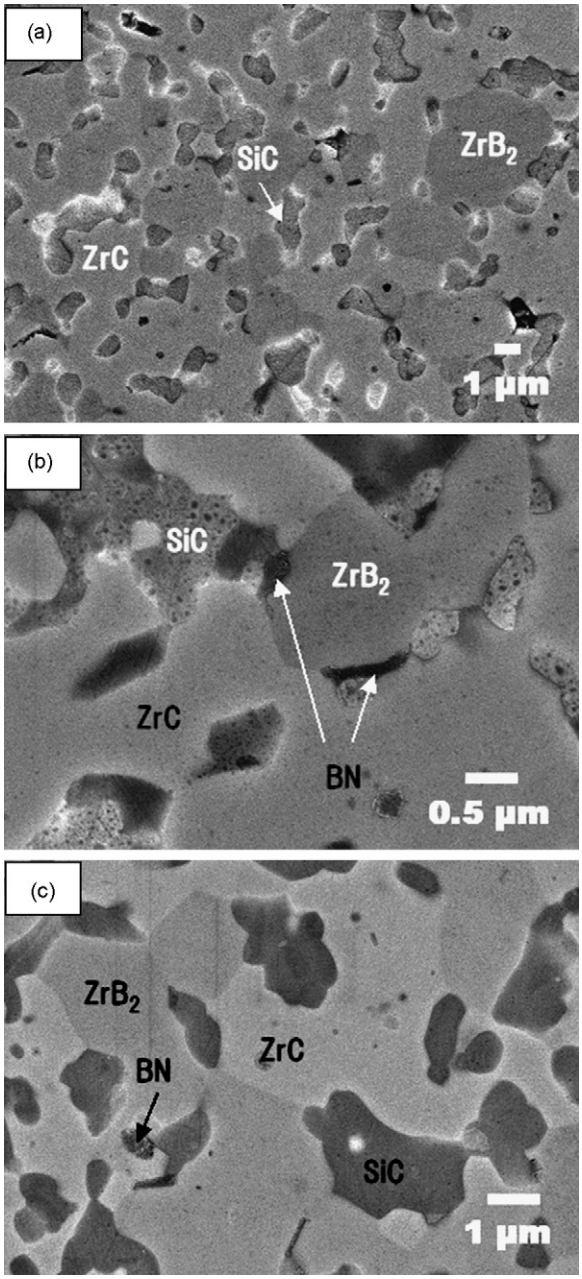

Fig. 3. FE-SEM images of the three compositions materials consolidated by SPS, (a) ZZS-4, (b) ZZS + AlN-4, and (c) ZZS + Si_3N_4-4.

$$B_2O_3 + 2AlN = 2BN + Al_2O_3 \quad (6)$$

$$2B_2O_3 + Si_3N_4 = 4BN + 3SiO_2 \quad (7)$$

The mentioned reactions are characterized by negative Gibbs free energy: −270 kJ/mol at room temperature for reaction (6) and −304 kJ/mol at 1500 °C for reaction (7). Similar reactions, although SPS instead of hot press, are expected for the ZrB_2–ZrC–SiC composites with AlN and Si_3N_4 additives investigated in this study. This suggests that AlN and Si_3N_4 are consumed during the sintering due to the mentioned reactions above leading to a complete disappearance of both additives in the X-ray reflections.

3.3. Elastic properties

The measured soundwave velocities and calculated elastic moduli for the three compositions investigated consolidated by SPS at various temperatures are summarized in Table 2. It is found that longitudinal and transverse soundwave velocities increased with density for the three compositions. This finding suggests that the soundwave velocities of the composite are closely linked to additives and porosity, because they may affect the measured density of the sintered composites. The effect of additives is stronger for the longitudinal soundwave velocity than for the transverse soundwave velocity. This suggests that the longitudinal soundwave is more sensitive to additives than the transverse soundwave. The largest value of the longitudinal soundwave velocity was measured in the fully dense ZZS + Si_3N_4 composite. Although this value is significantly larger than that of the ZZS + AlN composite, no significant difference was observed compared with the ZZS composite. On the other hand, the largest value of the transverse soundwave velocity was measured in the fully dense ZZS composite, and the value is significantly larger than that of the ZZS + AlN, but no significant difference was shown compared with the ZZS + Si_3N_4. The changes of the soundwave velocities with porosity are presented in Fig. 4. It is found that the soundwave velocities of the composites decreased linearly with porosity for every case. This indicated that the soundwave velocities strongly depended on the porosity in the materials. These results demonstrate that the soundwave velocities for an incompletely dense composite are mostly dominated by porosity. This is in consistence with Roth et al. [20], who showed a linear relation between the soundwave velocities measured and the volume fraction of porosity in the materials.

On the other hand, the calculated shear and the Young's moduli for the three compositions showed that the moduli linked with the additives and porosity (Table 2). However, Poisson's ratio is almost constant for the three compositions

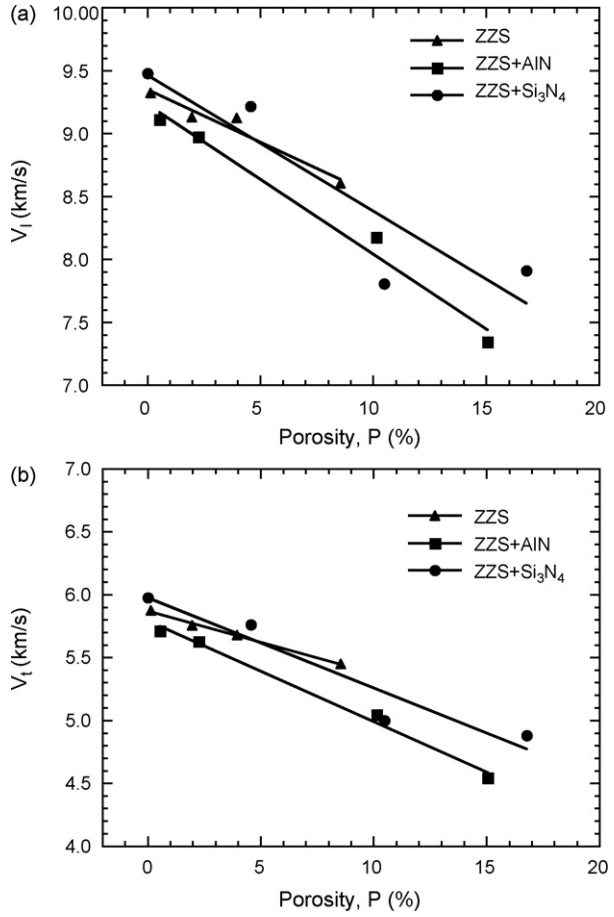

Fig. 4. Plots of the soundwave velocities vs. the porosity for the three composites consolidated by SPS: (a) longitudinal sound velocity, and (b) transverse sound velocity.

(Table 2), regardless of the additive and the porosity. This indicates that Poisson's ratio is insensitive to additives and pore content in the materials. The moduli for the fully dense ZZS and ZZS + Si_3N_4 composites are nearly the same, and they are significantly larger than those of the ZZS + AlN composite. For a full dense composite, Young's modulus of the composite, E_c, may be described by the rule of mixture as follows [21].

$$E_c = \sum_{i=1}^{n} E_i f_i \tag{8}$$

where E_i is Young's modulus of ith constituent phase, and f_i is volume fraction of ith constituent phase, and n is total number of constituent phases. With $E_1 = 540$ GPa (ZrB_2), $E_2 = 400$ GPa (ZrC), $E_3 = 480$ GPa (SiC) [22], $E_4 = 316$ GPa (AlN) [23], and $E_5 = 321$ GPa (Si_3N_4) [24], Eq. (8) yields $E_c = 454$, 442, and 440 GPa for the ZZS, ZZS + AlN, and ZZS + Si_3N_4, respectively. Obviously, for the ZZS the Young's modulus predicted is in agreement with the measured one. This agreement showed that the Young's modulus of pore-free ZZS composition obeyed the rule of mixture. For both the ZZS + AlN and ZZS + Si_3N_4 compositions, the Young's moduli predicted were inconsistent with those measured. This discrepancy may be attributed to the reactions of added AlN and Si_3N_4 with the B_2O_3 which is present on the surface of ZrB_2 particles.

The changes of the shear modulus and the Young's modulus with porosity for the three material compositions are presented in Fig. 5. The elastic moduli, including shear modulus and Young's modulus, for the three compositions decrease linearly with porosity. This strong relation demonstrates that the elastic moduli of the pores-containing composites are mostly dominated by the porosity of the materials. The empirical dependence of elastic moduli on porosity is reported in various materials. For ceramic materials, the linear empirical dependence has been recommended. Assuming that the effect of pore structure and shape on elastic moduli is neglected, the elastic moduli, M (G and E) can be given by [25].

$$M = M_0(1 - kP) \tag{9}$$

where M_0 is the elastic moduli (G and E) of pore-free materials, k a constant, and P is volume fraction of porosity in the materials. The M_0 and k values are obtained from the M–P plots shown in Fig. 5. The obtained data for the theoretical moduli, M_0, and the constants, k, are listed in Table 3. It is found that the elastic moduli of pore-free materials are the same for the ZZS + Si_3N_4 and ZZS composites being larger than that of the ZZS + AlN.

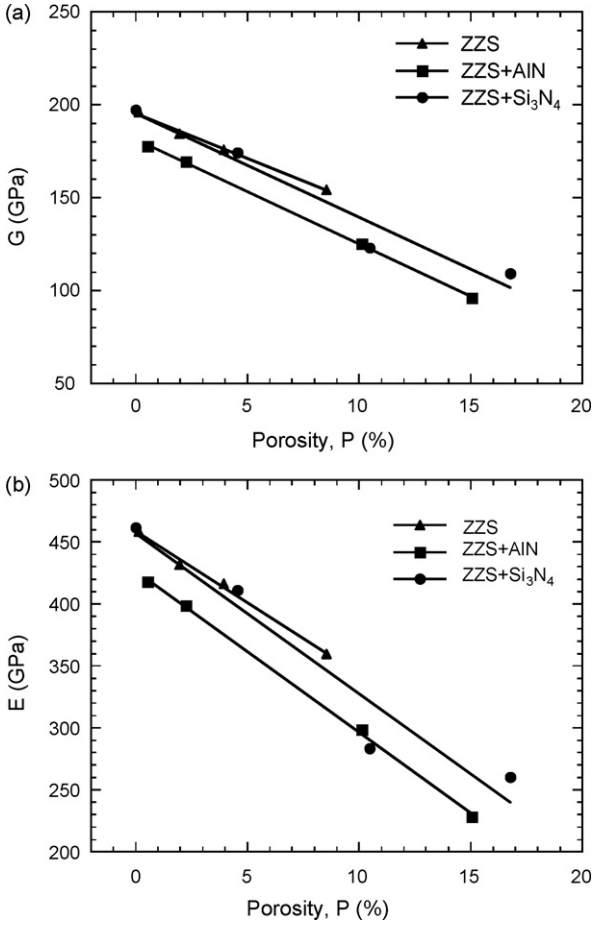

Fig. 5. Plots of the elastic moduli vs. the porosity for the three composites consolidated by SPS: (a) shear modulus, and (b) Young's modulus.

Table 3
The obtained theoretical elastic moduli for the three composites consolidated by SPS

Materials	Shear modulus, G (GPa)		Young's modulus, E (GPa)	
	G_0	g	E_0	e
ZZS	195	2.49	459	2.52
ZZS + AlN	182	3.11	427	3.05
ZZS + Si_3N_4	195	2.86	457	2.83

In Fig. 6, the change of the Young's modulus with longitudinal soundwave velocity for the three compositions is presented. It clearly shows that all the measured data points, regardless of their compositions and pressing route, lie along a line, showing very close correlation ($r^2 = 0.974$) between the Young's modulus and the longitudinal soundwave velocity. This linear correlation means that the Young's modulus of the composites strongly depended on the longitudinal soundwave velocity. The relationship between the Young's modulus and the longitudinal soundwave velocity was described by

$$E_c = E_0\left[1 - \beta\left(1 - \frac{V_l}{V_0}\right)\right] \quad (10)$$

where E_0 is the Young's modulus of the pore-free ZZS composite (=459 GPa, Table 3), β a constant and it is determined from Fig. 6 ($\beta = 2.35$), V_0 the longitudinal soundwave velocity of the pore-free ZZS material, and V_l is the longitudinal soundwave velocity measured in the ZZS materials with additives. This suggests that the Young's modulus of the materials could be predicted by the longitudinal soundwave velocity measured. This is in agreement with Yeheskel and Tevet [18], who showed a linear relation between the elastic modulus and the longitudinal soundwave velocity in hot isostatic pressing high purity Y_2O_3 and 10 mol% La_2O_3-strengthened Y_2O_3 ceramics materials.

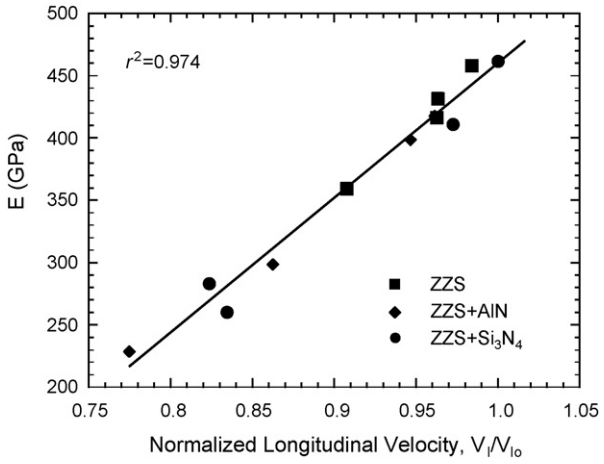

Fig. 6. Changes in the Young's modulus in the three composites consolidated by SPS vs. the normalized longitudinal soundwave velocity, showing a linear relationship between the Young's modulus and the sound velocity.

4. Summary remarks

Nearly-fully dense ZrB_2–ZrC–SiC (ZZS) composite was consolidated by spark plasma sintering at 1900 °C with a holding time of 5 min under a pressure of 30 MPa. The AlN and Si_3N_4 additives lowered the onset temperature of densification and promoted densification of the ZZS composites. This improvement was more significant for the AlN-containing ZZS than for the Si_3N_4-containing ZZS. The density exceeding of 97% was obtained at 1800 °C for the ZZS + AlN powder. The microstructure of the resulting composites was fine and homogenous for the three composites.

The elastic moduli of the ZrB_2–ZrC–SiC materials depended on the additives and porosity. The elastic moduli measured for the ZZS and ZZS + Si_3N_4 are nearly the same and they were higher than those of the ZZS + AlN. In addition, the elastic moduli of the three compositions lowered linearly with porosity. However, Poisson's ratio was almost constant for the studied materials, regardless of the additives and porosity. The obtained elastic moduli of the fully dense ZrB_2–ZrC–SiC materials with AlN and Si_3N_4 additives were the following: $E = 459$ GPa, $G = 196$ GPa, $\nu = 0.17$ for the ZZS, $E = 418$ GPa, $G = 178$ GPa, $\nu = 0.18$ for the ZZS + AlN, and $E = 462$ GPa, $G = 197$ GPa, $\nu = 0.17$ for the ZZS + Si_3N_4.

References

[1] K. Kuwabara, Some characteristics and applications of ZrB_2 ceramics, Bull. Ceram. Soc. Japan 37 (2002) 267–271.
[2] K. Upadhya, J.-M. Yang, W.P. Hoffmann, Materials for ultrahigh temperature structural applications, Am. Ceram. Soc. Bull. 76 (1997) 51–56.
[3] A.S. Brown, Hypersonic designs with a sharp edge, Aerospace Am. 35 (1997) 20–21.
[4] C. Mroz, Zirconium diboride, Am. Ceram. Soc. Bull. 73 (1994) 141–142.
[5] S. Norasetthekul, P.T. Eubank, W.L. Bradley, B. Bozkurt, B. Stucker, Use of zirconium diboride-copper as an electrode in plasma applications, J. Mater. Sci. 34 (1999) 1261–1270.
[6] R. Telle, L.S. Sigl, K. Takagi, Boride-based hard materials, in: R. Riedel (Ed.), Handbook of Ceramic Hard Materials, Wiley-VCH, Weinheim, Germany, 2000, pp. 803–945.
[7] A.K. Kuriakose, J.L. Margrave, Oxidation kinetics of zirconium diboride and zirconium carbide at high temperatures, J. Electrochem. Soc. 111 (1964) 827–831.
[8] W.C. Tripp, H.H. Davis, H.C. Graham, Effect of an SiC addition on the oxidation of ZrB_2, Am. Ceram. Soc. Bull. 52 (1973) 612–616.
[9] F. Monteverde, A. Bellosi, Effect of the addition of silicon nitride on sintering behavior and microstructure of zirconium diboride, Scripta Mater. 46 (2002) 223–228.
[10] F. Monteverde, A. Bellosi, Development and characterization of metal-diboride-based composites toughened with ultra-fine SiC particulates, Solid State Sci. 7 (2005) 622–630.
[11] F. Monteverde, A. Bellosi, Beneficial effects of AlN as sintering aid on microstructure and mechanical properties of hot-pressed ZrB_2, Adv. Eng. Mater. 5 (2003) 508–512.
[12] M. Nygren, Z. Shen, On the preparation of bio-, nano- and structural ceramics and composites by spark plasma sintering, Solid State Sci. 5 (2003) 125–131.
[13] M. Nygren, Z. Shen, Novel assemblies via spark plasma sintering, Silic. Indus. 69 (2004) 211–218.
[14] V. Medri, F. Monteverde, A. Balbo, A. Bellosi, Comparison of ZrB_2–ZrC–SiC composites fabricated by spark plasma sintering and hot-pressing, Adv. Eng. Sci. 7 (2005) 159–163.

[15] A. Bellosi, F. Monteverde, D. Sciti, Fast densification of ultra-high-temperature ceramics by spark plasma sintering, Int. J. Appl. Ceram. Technol. 3 (2006) 32–40.
[16] K.A. Khor, K.H. Cheng, L.G. Yu, F. Boey, Thermal conductivity and dielectric constant of spark plasma sintered aluminum nitride, Mater. Sci. Eng. A347 (2003) 300–305.
[17] M. Brach, D. Sciti, A. Balbo, A. Bellosi, Short-term oxidation of a ternary composite in the system of AlN–SiC–ZrB_2, J. Euro. Ceram. Soc. 25 (2005) 1771–1780.
[18] O. Yeheskel, O. Tevet, Elastic moduli of transparent yttria, J. Am. Ceram. Soc. 82 (1999) 136–144.
[19] S.Q. Guo, N. Hirosaki, Y. Yamamoto, T. Nishimura, M. Mitomo, Hot-press sintering silicon nitride with Lu_2O_3 addition: elastic moduli and fracture toughness, J. Euro. Ceram. Soc. 23 (2003) 537–545.
[20] D.J. Roth, D.B. Stang, S.M. Swickard, M.R. DeGuire, NASA Rept. No. NASA-TM-102501, March 1990.
[21] R.W. Rice, Particle effects on elastic properties, crack propagation and fracture toughness of ceramic composites at ∼22 °C, in: Mechanical Properties of Ceramics and Composites, Marcel Dekker, Inc., New York, 2000, p. 457.
[22] H. Holleck, Material selection for hard coatings, J. Vac. Sci. Technol. 4 (1986) 2661–2669.
[23] W.S. Cho, M.W. Cho, J.H. Lee, Z.A. Munir, Effects of h-BN additive on the microstructure and mechanical properties of AlN-based machinable ceramics, Mater. Sci. Eng. A418 (2006) 61–67.
[24] T. Rouxel, J.C. Sangleboeuf, M. Huger, C. Gault, J.L. Besson, S. Testu, Temperature dependence of Young's modulus in Si_3N_4-based ceramics: roles of sintering additives and Si-particle content, Acta Mater. 50 (2002) 1669–1682.
[25] E.A. Dean, J.A. Lopez, Empirical dependence of elastic moduli on porosity for ceramic materials, J. Am. Ceram. Soc. 66 (1983) 366–370.